



Numerical analysis of single and multiple particles of Belchatow lignite dried in superheated steam

Marcin Zakrzewski^{1,2} · Anna Sciazko^{1,3} · Yosuke Komatsu³ · Taro Akiyama⁴ · Akira Hashimoto³ · Shozo Kaneko³ · Shinji Kimijima⁵ · Janusz S. Szmyd¹ · Yoshinori Kobayashi³

Received: 10 April 2017 / Accepted: 16 February 2018 / Published online: 8 March 2018
© The Author(s) 2018. This article is an open access publication

Abstract

Low production costs have contributed to the important role of lignite in the energy mixes of numerous countries worldwide. High moisture content, though, diminishes the applicability of lignite in power generation. Superheated steam drying is a prospective method of raising the calorific value of this fuel. This study describes the numerical model of superheated steam drying of lignite from the Belchatow mine in Poland in two aspects: single and multi-particle. The experimental investigation preceded the numerical analysis and provided the necessary data for the preparation and verification of the model. Spheres of 2.5 to 30 mm in diameter were exposed to the drying medium at the temperature range of 110 to 170 °C. The drying kinetics were described in the form of moisture content, drying rate and temperature profile curves against time. Basic coal properties, such as density or specific heat, as well as the mechanisms of heat and mass transfer in the particular stages of the process laid the foundations for the model construction. The model illustrated the drying behavior of a single particle in the entire range of steam temperature as well as the sample diameter. Furthermore, the numerical analyses of coal batches containing particles of various sizes were conducted to reflect the operating conditions of the dryer. They were followed by deliberation on the calorific value improvement achieved by drying, in terms of coal ingredients, power plant efficiency and dryer input composition. The initial period of drying was found crucial for upgrading the quality of coal. The accuracy of the model is capable of further improvement regarding the process parameters.

Keywords Superheated steam drying · Low-rank coal · Multi-particle drying · Numerical simulation · Fuel upgrading · Belchatow lignite

✉ Marcin Zakrzewski
marcin.zakrzewski@agh.edu.pl

¹ Faculty of Energy and Fuels, Department of Fundamental Research in Energy Engineering, AGH University of Science and Technology, 30 Mickiewicza Avenue, 30-059 Krakow, Poland

² Graduate School of Engineering and Science, Division of Regional Environment Systems, Shibaura Institute of Technology, 307 Fukasaku, Minuma-ku, Saitama-shi, Saitama 337-8570, Japan

³ Institute of Industrial Science, The University of Tokyo, 4-6-1 Komaba, Meguro-ku, Tokyo 153-8505, Japan

⁴ Fudo Giken Industry Co. Ltd., 2-6-30 Niihama, Arai-chou, Takasago-shi Hyogo, Japan

⁵ College of Systems Engineering and Science, Department of Machinery and Control Systems, Shibaura Institute of Technology, 307 Fukasaku, Minuma-ku, Saitama-shi, Saitama 337-8570, Japan

Nomenclature

Symbols:

b	Half of layer's thickness [m]
B	Uniformity constant for coal particle distribution equation [-]
c	Specific heat [$\text{J kg}^{-1} \text{ }^\circ\text{C}^{-1}$]
$\{CO_2\}$	Unit emission of carbon dioxide [kg kg^{-1}] or [kg kWh^{-1}]
d	diameter [m]
D	Diffusion coefficient of free water [$\text{m}^2 \text{ s}^{-1}$]
E	Electricity generation per fuel mass unit [kWh kg^{-1}]
h	Heat transfer coefficient [$\text{W m}^{-2} \text{ }^\circ\text{C}^{-1}$]
ΔH	Enthalpy change of bound water evaporation [J kg^{-1}]
HHV	Higher heating value [J kg^{-1}]
η	Thermal efficiency [%]
λ	Thermal conductivity [$\text{W m}^{-1} \text{ }^\circ\text{C}^{-1}$]
L	Latent heat of free water [J kg^{-1}]

LHV	Lower heating value [$J\ kg^{-1}$]
m	Mass [kg]
\mathbf{n}	Normal vector
N	Number of layers within a lignite sphere
\dot{q}_V	Volumetric heat sink [$W\ m^{-3}$]
ΔQ	Heat input/consumption [J]
r	Radius [m]
ρ	Density [$kg\ m^{-3}$]
t	Time [s]
Δt	Time step [s]
T	Temperature [$^{\circ}C$]
ΔT	Change of temperature [$^{\circ}C$]
V	Volume [m^3]
WP	Water percentage [mass%]
WS	Water share [mass%]
X	Moisture content [–]

Sub- and superscripts:

a	Superheated steam
b	Bulk
ad	Air-dried coal
apr	Approximated
avg	Average
c	Dry coal
CDRP	Constant drying rate period
cond	Condensation
cons	Consumption
d	Dried coal
dry	Drying
evap	Evaporated water
exp	Experimental
free	Referring to free water
i	Time instance
ini	Initial
n	Referring to n -th layer
raw	As-received coal
s	Surface
trans	Water transfer
w	Water

1 Introduction

Lignite (also known as brown coal) has a vital position in a number of power generation systems, particularly in Europe. Shallow deposits of this widely distributed resource are cheap in extraction, therefore the total cost of electricity generation in lignite-fired power plants is relatively low [1]. On the other hand, coalification processes did not develop as much as in the case of bituminous coal, what negatively influenced the elemental carbon share in brown coal. Unfortunately, in terms of power generation applicability, water content often prevails over combustible matter, what undermines the calorific value of this energy carrier. The occurrence of water also makes transportation and

storage economically unjustified. Yet, the aforementioned low production costs combined with significant volatile matter share, which boosts gasification potential, makes upgrading the quality of lignite by drying worthy of consideration.

The key aspect of drying in any technological process is maximization of the ratio between the achieved increase in material quality (measured by the expiration date, water percentage, calorific value etc. [2–4]) and the heat consumed by the drying system. Superheated steam drying is one of the prospective methods, promising the possibility of latent heat recovery, what might considerably reduce the heat demand of fuel preparation devices.

This drying medium has been discussed since the early twentieth century [5] and its application as an alternative to hot air for dewatering granular objects was proposed in 1951 [6]. The advantages of superheated steam drying include the reduction of spontaneous ignition hazard and, above a certain temperature, higher drying efficiency than hot air [7]. The key benefit, though, is the capability for latent heat recovery. One of the applications realizing such an idea is the superheated steam fluidized bed dryer [8, 9]. In this concept, the drying system operating in a self-heat recuperation configuration enables the collection of steam from the moisture in the raw fuel, followed by the recirculation of its latent and sensible heat for the drying of another fuel portion [10, 11]. By that means, the heat of the phase transition is not given off to the ambience, what results in the decline of energy consumption, thus elevating the thermal efficiency of the system.

The reliable approach to the design and construction of a superheated steam drying (SSD) system coupled with a power generation unit, entails a thorough study on fuel taken into consideration. This kind of works often include numerical analysis as a cheap and precise manner of describing heat and mass transfer phenomena which occur in the drying process. The food industry has commonly adapted such a method of drying optimization. The model of fixed bed dryer of brewers' spent grain using superheated steam one of the examples [12]. Applying the finite difference method, changes in moisture content and temperature in the slice of pork were simulated for SSD [2]. Power engineering also reached for the superheated steam drying models, what resulted in the numerical analysis of the combined heat and power plant fueled by corn ethanol [4] as well as the self-heat recuperative fluidized bed dryer of biomass, which consumed 95% less energy than conventional systems [3]. Coal became the object of drying simulations with regard to its granular form [13]. Another study [14] came out with a single particle SSD model prepared for Australian lignite from the Loy Yang mine. The work was followed by a simulation of multi-object drying [15]. The experimental methodology of the two last mentioned works was analogical as in this study.

A previously verified [16] numerical model of superheated steam drying of Belchatow lignite was applied to this study, relying on the experimental research conducted beforehand on the drying characteristics of Polish lignite

excavated from the Belchatow deposit. Outcomes acquired from the drying of variously sized objects is applied in this study to numerically analyze multi-particle SSD, which can reflect the actual operation mode of a dryer more precisely. The simulation is utilized to evaluate the potential of calorific value enhancement, including diverse scenarios of input composition and its influence on the performance of the superheated steam dryer.

2 Experimental methodology

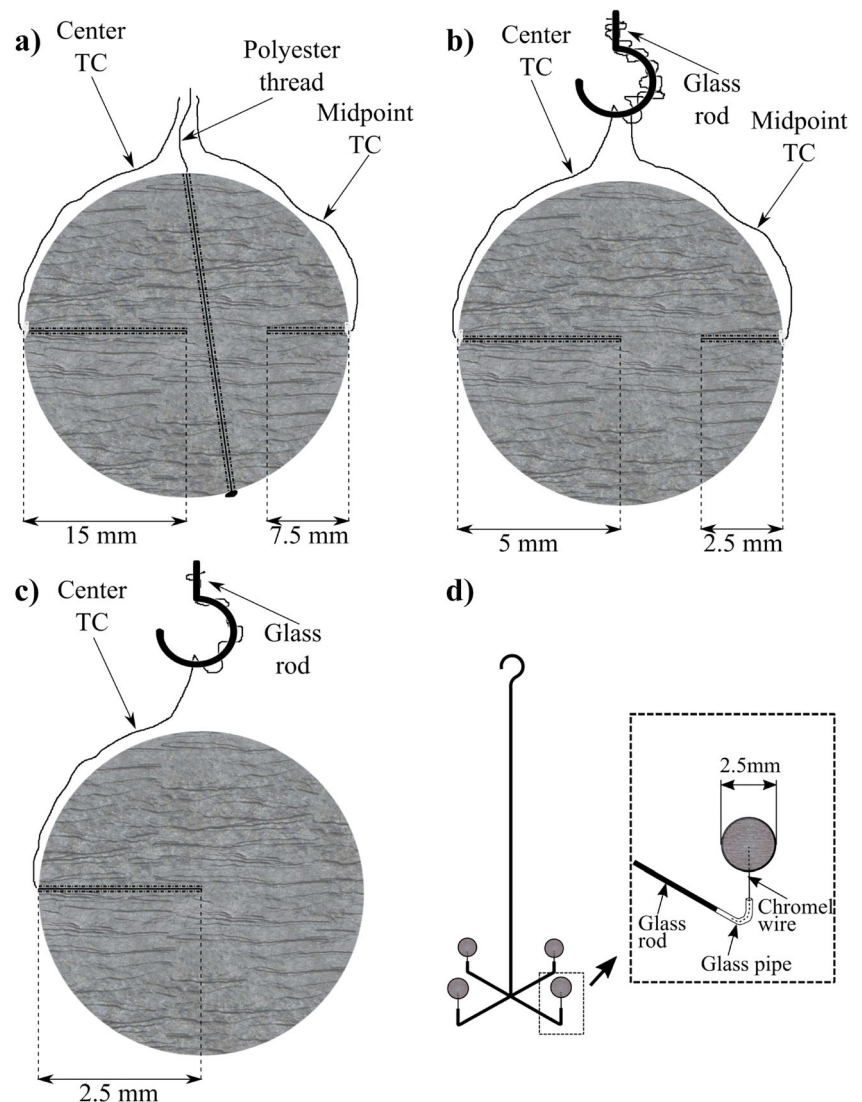
2.1 Samples

Spherical objects of four diameters were included in the examination: 30, 10, 5 and 2.5 mm. The investigated material originated in the Belchatow lignite mine and was excavated in a batch denominated B2013. Each sample

type was prepared by rolling a piece of lignite on a plate with a series of punctuated holes, which diameter declined stepwise to the demanded size. The particles of various sizes differed in methods of suspension inside the test section and the temperature measurement.

Figure 1 presents the lignite samples together with the installation methods. Particles of 30 (Fig. 1a) and 10 mm (Fig. 1b) were equipped with two thermocouples per each, measuring temperatures in the half of the radius (later called “midpoint”) and the center. The other function of the thermocouples was the suspension of the sphere in the experimental vessel, however, the largest sample was additionally stabilized with polyester thread passed through its interior. One thermocouple, measuring temperature in the center, was placed in the object of 5 mm (Fig. 1c). In the case of 2.5 mm (Fig. 1d) no thermocouple was applied and a quadruple glass hanger was used to suspend the four samples at a time.

Fig. 1 Samples of a) 30, b) 10, c) 5, d) 2.5 mm with characteristic equipment



2.2 Setup and procedure

The scheme of the experimental apparatus is presented in Fig. 2. Before the tests, the examined sphere (or spheres) was inserted into the test cylinder, which was heated and insulated in order to assure the thermal stability. The distilled water was used to generate superheated steam. It was degassed, pumped to an evaporator, turned to steam and then superheated. The gaseous medium filled the test vessel through a baffle plate, used for the uniform distribution of steam within the chamber. The input rate of the water into pump and degasser was $8 \text{ cm}^3 \text{ min}^{-1}$.

The temperature of the steam varied between 110 and 170 °C, depending on the test case, while its pressure was kept at 1 atmosphere. The assumptions of water condensation and coal volatilization limited the temperature range from the bottom and top, respectively. The decomposition of lignite structure was not observed [17] below 180 °C, hence the water removal is treated as an exclusive reason for the descent of the sample weight.

The temperature measurement of the coal interior was realized depending on the particle diameter, as mentioned in the previous subsection. Moreover, an independent measurement of coal surface temperature was conducted by means of thermography for objects of all sizes. The electronic balance with a metal rod, on which the lignite was suspended, enabled the weight measurement. The completion of steam drying was followed by the substitution of medium to nitrogen, which was applied to remove the residual water within the coal. More details of the experimental procedure, with respect to each type of examined object, are given in the previous works [18–20].

2.3 Drying indicators

Relying on the mass of the sample after the completion of nitrogen drying, two parameters, applied for quantitative

description of the drying process, were calculated. They are introduced below.

Moisture content X , is expressed as a ratio of water mass in coal (variable in time) to the mass of the dry coal remaining after drying. The formula is given in Eq. 1:

$$X^i = \frac{m_w^i}{m_c} \tag{1}$$

Water percentage WP , represents the share of the water in the lignite sample, related to the initial mass of the sample. It is formulated as mass percentage and shown in Eq. 2:

$$WP^i = \frac{m_w^i}{m^0} \cdot 100 = \frac{m_w^i}{m_w^0 + m_c} \cdot 100 \tag{2}$$

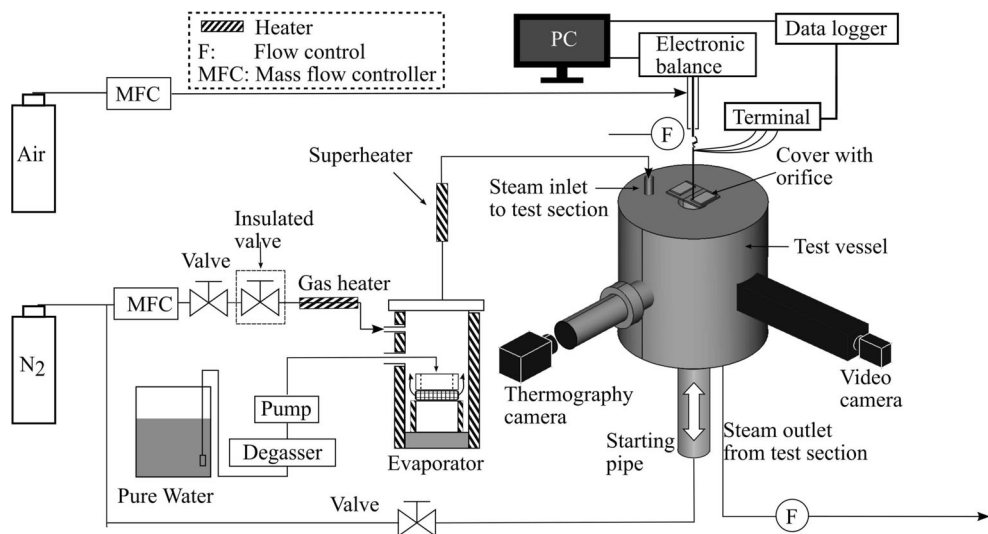
3 Model of superheated steam drying

3.1 Physical model

The physical model of drying was assumed to be a sphere, comprising of three phases of different thermophysical properties: dry coal matter, free water and bound water. Dry coal matter represents the solid mixture of carbon, carbohydrates and ash that are not subject to evaporation and therefore their total mass does not vary through the drying process. Free water is assumed to evaporate at saturation temperature, which is 100 °C under atmospheric pressure, while bound water turns to steam above this temperature.

The model was constructed on the assumption that the object is a perfect sphere of isotropic properties. The parameters of dry coal, such as density ρ_c , specific heat c_c or thermal conductivity k_c , are constant during drying. On the other hand, the analogical properties of water are significantly dependent

Fig. 2 Scheme of the experimental setup



on temperature, so the empirical formulas need to be applied as the temperature increases. Moreover, evaporation and diffusion alter the moisture content in the lignite interior (along the radius), what impacts the resultant values of particular properties.

The significantly important parameters for conducting this study are given in Table 1. For the purpose of simulation, some physical and chemical properties, due to the lack of proper data on Belchatow coal, were adapted from other lignite types. A few of them were derived directly for Belchatow, based on empirical data, found in an auxiliary investigation or acquired from commissioned research.

3.2 Mathematical model

Due to the above-mentioned isotropy of the properties, a one-dimensional model of transient heat transfer, along the sample radius, might be applied. The formula describing the temperature field under those conditions, is given by Eq. 3:

$$c(r, t)\rho(r, t) \frac{\partial T(r, t)}{\partial t} = \nabla \cdot (\lambda(r, t) \nabla T) - \dot{q}_V \quad (3)$$

where \dot{q}_V stands for the volumetric heat sink represents heat loss by the evaporation of free and bound water (Section 3.3.3.). The first component of the right-hand side of Eq. 3 can also be expressed in that case as:

$$\nabla \cdot (\lambda(r, t) \nabla T) = \frac{1}{r^2} \frac{\partial}{\partial r} \left[r^2 \lambda(r, t) \frac{\partial T(r, t)}{\partial r} \right] \quad (4)$$

The initial condition is:

$$T(r, t)|_{t=0} = T^0 = 40^\circ \text{C} \quad (5)$$

The boundary conditions reflect the symmetry condition and the transfer of heat from the steam to the surface of a sample, respectively:

$$\frac{\partial T(r, t)|_{r=0}}{\partial r} = 0 \quad (6)$$

$$-\lambda \frac{\partial T(r, t)|_{r=r_1}}{\partial r} = h(r_1, T_a)[T_a - T_1(t)] \quad (7)$$

Heat transfer coefficient h in Eq. 7 is a function of the steam temperature (the surrounding space around the sample is fulfilled with steam) and sample diameter. It was previously derived relying on thermodynamic deliberation on superheated steam drying, performed for the same lignite type [18]. The used formula is given in Table 1.

Whether the moisture content X_n in layer n is higher than equilibrium moisture content X_{eq} in the current temperature (see Table 1), the diffusion of water to the layer $n-1$ occurs. The mass flow is governed by the Fick's law:

$$\dot{m}_w = -DA \frac{\partial \rho_{b,w}}{\partial r} \quad (8)$$

where $\rho_{b,w}$ is a bulk density or mass concentration of water within lignite and D , which value is given in Table 1, stands for diffusion coefficient of free water [14].

3.3 Numerical model

3.3.1 Discretization scheme

In order to transform the differential equations into algebraic formulas, the control-volume method was applied

Table 1 Selected properties of coal applied in the simulation (lignite types: B – Belchatow, Y – Yallourn, LY – Loy Yang)

Parameter	Lignite	Value	Source
initial moisture content X^0	B	1.05	experimental average, equal to WS = 51.25%
specific heat (dry coal) c_c	B	1246 J kg ⁻¹ °C ⁻¹	commissioned research
thermal conductivity (dry coal) λ_c	B	0.33 W m ⁻¹ °C ⁻¹	auxiliary in-house tests
heat transfer coefficient h from superheated steam with temperature T_a [°C] to spherical particle of diameter d [m]	B	$(2.38 \times 10^{-4}/d - 9.17 \times 10^{-2}) \times T_a - (3.52 \times 10^{-4}/d - 19.63)$ W m ⁻² °C ⁻¹	thermodynamically derived in [18]
equilibrium moisture content X_{eq}	Y	$0.71/(T_n - 98.58) + 0.06$	in range 100–114.1 °C, adapted from [14]
	B	$4.77 \times \exp.[2.36 \times (T_n - 100)^{0.18}]$	in range 114.1–170 °C, experimental data
enthalpy change of bound water evaporation ΔH	Y	$2.93 \times 10^6 - 6.76 \times 10^5 \times \exp.[-0.08 \times (T_n - 100)]$ J/kg	adapted from [14]
linear shrinkage $1 - l/l_{ini}$	LY	$-0.27 \times (V_w/V_w^0)^3 + 0.66 \times (V_w/V_w^0)^2 - 0.55 \times (V_w/V_w^0) + 0.16$	adapted from [14]
diffusion coefficient of free water D	LY	3.0×10^{-9} m s ⁻²	adapted from [14]

[21, 22]. Assuming element n within a sphere, which volume is V_n and area equals to A_n , Eq. 3 can be integrated on this element as:

$$\int_{V_n} c(r, t)\rho(r, t) \frac{\partial T(r, t)}{\partial t} dV = \int_{V_n} \nabla \cdot (\lambda(r, t) \nabla T) dV - \int_{V_n} \dot{q}_V dV \tag{9}$$

The first component of right-hand side in Eq. 9 is equal to:

$$\int_{V_n} \nabla \cdot (\lambda(r, t) \nabla T) dV = \int_{A_n} \mathbf{n} \cdot (\lambda(r, t) \nabla T) dA \tag{10}$$

where \mathbf{n} is a normal vector.

Density ρ_n , thermal conductivity λ_n and specific heat c_n are assumed to be constant over the entire element n . Therefore, the apparent values dependent of volume fraction of coal and steam in each time step are used in the calculation domains, so Eqs. 9 and 10 might be integrated to:

$$\int_{V_n} c(r, t)\rho(r, t) \frac{\partial T(r, t)}{\partial t} dV = V_n \rho_n c_n \frac{\partial T_n}{\partial t} \tag{11}$$

and:

$$\int_{A_n} \mathbf{n} \cdot (\lambda(r, t) \nabla T) dA = \sum (\dot{Q}_{in,n} - \dot{Q}_{out,n}) \tag{12}$$

where the right-side of Eq. 12 represent heat fluxes by the conduction driven into and out of layer n .

As to the mass diffusion between the layers, integration of Eq. 8 from r_n to r_{n+1} gives:

$$\dot{m}_{in,n} = D \frac{4\pi r_n r_{n+1} \rho_{b,c,n} (X_{n+1} - X_n)}{r_n - r_{n+1}} \tag{13}$$

3.3.2 Particular discretization assumptions

Besides those introduced in the previous section, the following assumptions related to the discretization need to be listed:

- The uniform spatial distribution of the elements along the radius was applied, forming a series of concentric layers characterized with an initial width equal to $2b$. Only the initial width of extreme elements, number 1 and $N + 1$, was equal to b in order to avoid overlapping of the control-volume balances (Fig. 3).
- The sample division N was chosen to be 50, what ensures the accuracy of the numerical prediction independent from the grid size of the computational domain.

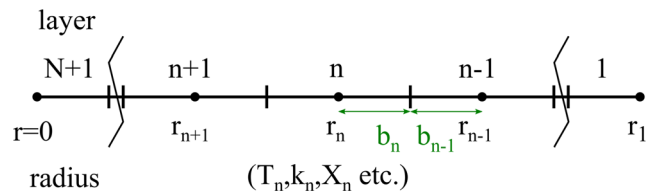


Fig. 3 Distribution of elements within a lignite sphere

- The simulation was performed using the explicit method with a specific value of the time step width Δt adjusted to the conditions:

$$\Delta t < \frac{(\Delta x)^2}{2\alpha} \tag{14}$$

By default, Δt was equal to 10^{-3} s, nonetheless it was set at 10^{-4} s for samples smaller than 2.5 mm in diameter and for objects of diameter smaller than 1 mm it was 10^{-5} s.

3.3.3 Specificity of particular drying stages

During the drying process, the mechanisms of heat and mass transfer vary, with the occurrence of water and temperature level as the main criteria. The numerical model, prepared with regard to the assumptions pointed out in sections 3.1–3.3 was structurally segmented with respect to the mechanism of dewatering. Consecutive drying stages, characterized with various sets of numerical equations, are described in the following subsections. However, the heat conduction between adjacent layers was a common mechanism for all stages and is presented by Eq. 15.

$$\Delta Q_n^{i+1} = \frac{4\pi r_{n,out}^i}{b_{n-1}^i / (\lambda_{n-1}^i, r_{n-1}^i) + b_n^i / (\lambda_n^i, r_n^i)} (T_{n-1}^i - T_n^i) \Delta t \tag{15}$$

Condensation of water on the surface The temperature of the sample in the initial stage of drying is lower than the saturation temperature. That is why, a condensation of water occurs on the coal surface. The total heat input to the dried object is covered by this mechanism, what is reflected by Eq. 16:

$$\Delta Q_1^{i+1} = h_{cond} 4\pi (r_1^0)^2 (100 - T_s^i) \Delta t \tag{16}$$

The heat consumed at that time causes the increase in the temperature of the dry coal and moisture within the sphere.

$$\Delta Q_{cons,n}^{i+1} = \left(c_c m_{c,n} + c_w^i m_{w,n}^i \right) \Delta T_n^i \tag{17}$$

Evaporation of water from the surface As the temperature of the surface of the coal sample reaches 100 °C, heat transfer to the sample becomes proportional to the temperature difference between the superheated steam and saturation

temperature of water remaining in the sample, what is presented in Eq. 18.

$$\Delta Q_1^{i+1} = h4\pi(r_1^i)^2(T_a - 100)\Delta t \quad (18)$$

The heat transfer coefficient applied to this period was evaluated relying on the mass evaporated during the constant drying rate period, as shown in Eq. 7. Then, it was linearized in the form of function, of which the variables are the temperature of the superheated steam and the reciprocal of the sample diameter, as seen in Table 1. In this stage of drying, the water film formed by condensation and exudation, remained on the surface. In the case of the larger samples it tended to exceed the critical mass and a part of it fell down in the form of droplets. The assumptions beyond the droplet formation were adapted from another study [15].

Evaporation of free water The mechanism beyond heat transfer to the sample surface does not change after the removal of water from the surface, however, heat input becomes proportional to the difference between the gas temperature and current temperature, which exceeds 100 °C and gradually increases (Eq. 19).

$$\Delta Q_1^{i+1} = h4\pi(r_1^i)^2(T_a - T_s^i)\Delta t \quad (19)$$

Free water in coal, similarly to water on the surface, evaporates at saturation temperature. The relation between heat consumed by the layer and the mass of water evaporated from it can be formulated as:

$$\Delta Q_{\text{cons},n}^{i+1} = \Delta m_{\text{evap},n}^i L \quad (20)$$

Due to evaporation of water, the moisture content gradient occurs between the layers. The gradient induces water transport between the layers. The bulk density of the water may be expressed as:

$$\rho_{\text{b},w,n} = \frac{m_{w,n} m_{c,n}}{V_n m_{c,n}} = \frac{m_{w,n} m_{c,n}}{m_{c,n} V_n} = X_n \rho_{\text{b},c,n} \quad (21)$$

Taking formula 21 into account, the transfer mechanism of free water, is illustrated by Eq. 22.

$$\Delta m_{\text{trans},in,n}^{i+1} = -D\rho_c 4\pi r_n^i r_{n+1}^i \frac{X_n^i - X_{n+1}^i}{b_n^i + b_{n+1}^i} \Delta t \quad (22)$$

Evaporation of bound water When the temperature of a particular layer exceeds 100 °C, it signals that free water evaporation is over and bound water only remains in the coal sample. Bound water is held firmly within the lignite structure, therefore its evaporation poses a greater challenge than the removal of free water. The evaporation rate at a certain moment is limited, therefore a surplus of heat input is allocated on

raising the temperature. Instead of the simple kinetic of latent heat consumed in the evaporation mechanism, an enthalpy change of bound water evaporation which can be described as the function of the layer temperature, applies at that stage. The heat consumption during bound water evaporation is presented in Eq. 23.

$$\Delta Q_{\text{cons},n}^{i+1} = \left[c_c m_{c,n} + c_{w,n}^i (m_{w,n}^i - \Delta m_{\text{evap},n}^i) \right] \Delta T_n^i + \Delta m_{\text{evap},n}^i \Delta H_n^i \quad (23)$$

The observation of the sample appearance indicated a considerable shrinkage phenomenon below the moisture content of around 0.6 [23]. Such a value is characteristic for the stages of drying when the surface temperature is over 100 °C, what means bound water is being evaporated from the shallow parts of the coal. Hence, the shrinkage equation, dependent on the moisture content, was implemented to modify the particle size during simulation, as presented in Table 1.

4 Results and discussion

4.1 Simulation of single particle drying in superheated steam

4.1.1 Comparison of empirical and numerical results

The simulation results were put together with the experimental data in Fig. 4. The changes in the moisture content, the drying rate (which is a time derivative of the moisture content) and the temperature profiles (surface and center) were included in the drying characteristics. Midpoint temperatures were neglected on purpose due to the clarity of the presented graphs. The comparison was made for 10 mm samples, exposed to the steam at the entire temperature range. The empirical results were appropriated from the previous study [16]. The simulation was conducted for the initial water percentage agreed in each case with the experimental value in order to check the coherence of the results. The other independent variables, in particular those indicated in Table 1 remained unaffected for all instances.

Concluding from the charts, a high temperature of the superheated steam entailed the elevated speed of drying. For that reason, water from lignite was discarded sooner and the sample reached thermal equilibrium with the steam, reducing the time required for the completion of the process.

The rise of the temperature, especially in the case of the temperature at the center of the sample, was more gradual for the experimental results and it occurred sooner than the time predicted by the simulation. Moreover, the apparent distinction between the surface and center temperature predicted

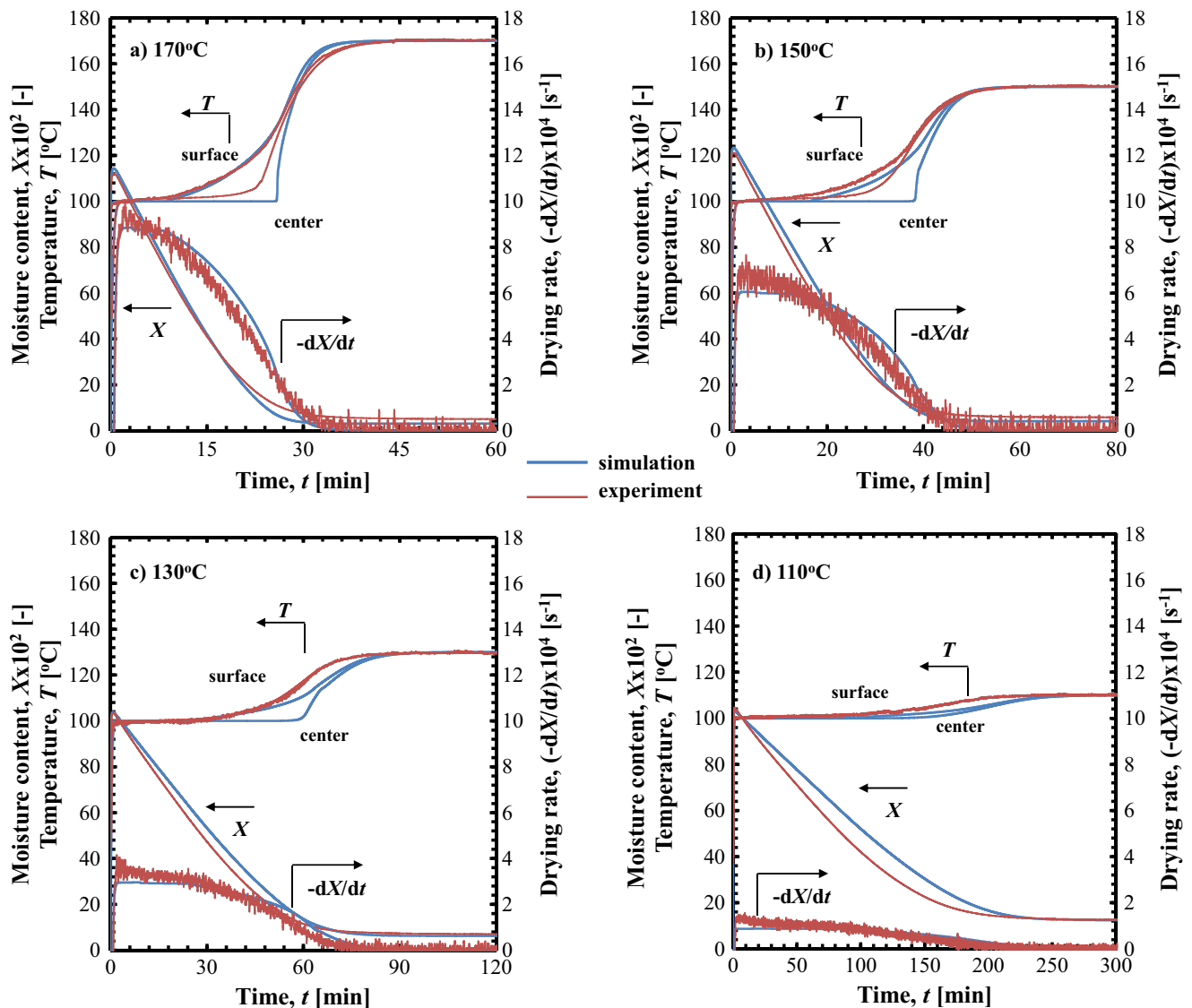


Fig. 4 Simulated values (blue) of 10 mm sample drying characteristics compared to experimental results (red) at test temperatures of a) 170, b) 150, c) 130 and d) 110 °C

numerically, does not occur in the experiments with the exception for a) and b) instances. The model adapted in this study assumed the increase of the temperature over 100 °C in the particular layer only after the complete removal of the free water in this layer. Uniformity of structure within the lignite and deformations occurring in the drying process may influence the boundary between the free and bound water moved at various paces within the different cross-sections, and made the temperature profile inconsistent with the calculated prediction as seen in Fig. 4.

Similarly to the set of results presented for the particular diameter, another one was prepared for the temperature fixed at 150 °C and a wide range of sizes. It is illustrated in Fig. 5. Note that due to a lack of interior temperature measurement, only one experimental curve

representing the surface is given in the temperature profile of the 2.5 mm sample chart.

The major disparity is visible in the time and speed of drying, however, the trends followed by the corresponding curves are alike. The oscillations on the drying rate experimentally obtained, are enhanced with the decrease in diameter and are resulted from the precision of the electronic balance (0.1 mg), which influences the smaller objects to a greater degree. In the case of Fig. 5a) the predicted drying rate slightly overshoots the empirical level, unlike the other cases, but the agreement between the analogical parts of the temperature profile seems the most precise. The same observations apply to the instance of 170 °C in Fig. 4a). The issue requires further improvements, including deliberation on the empirically obtained

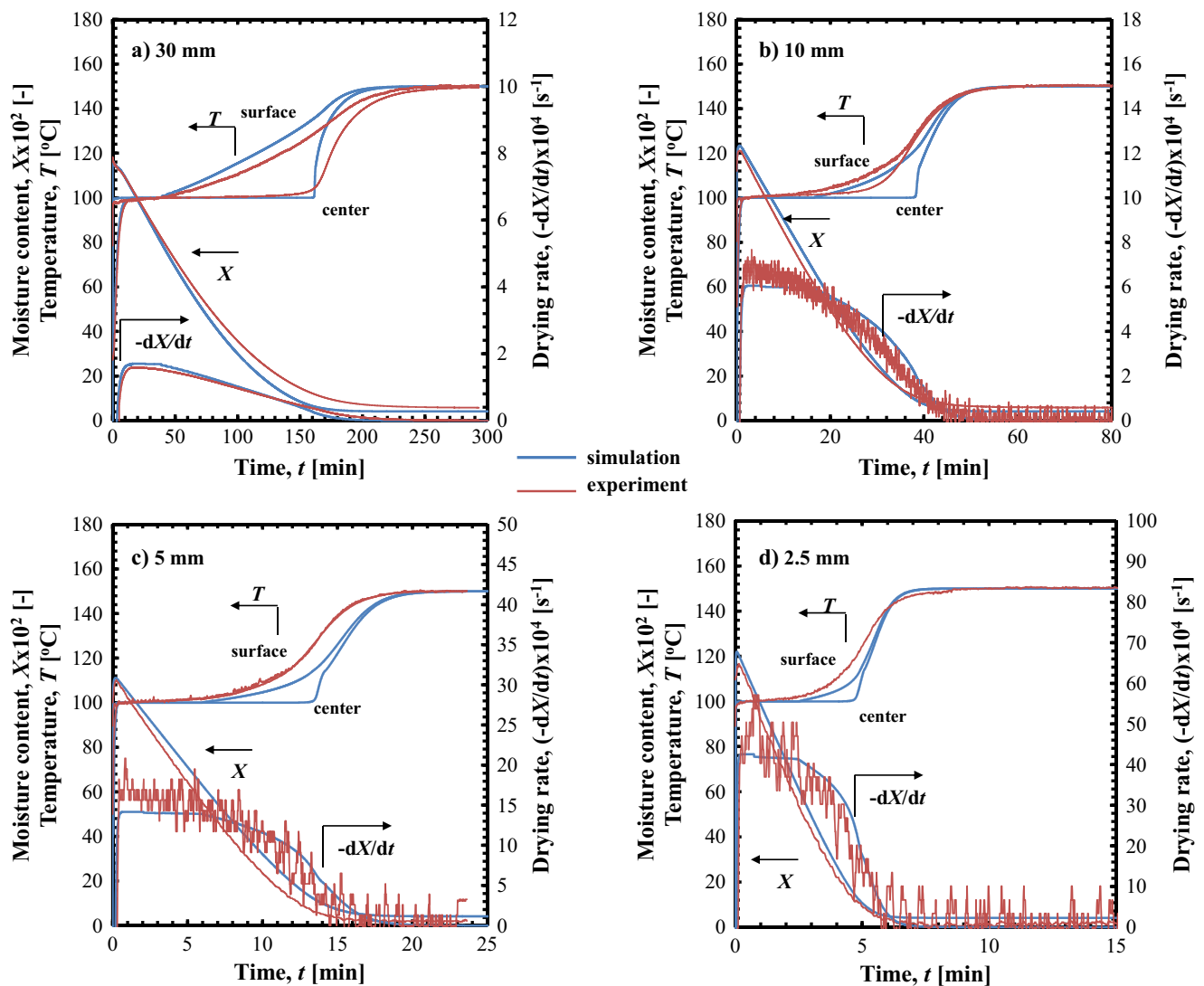


Fig. 5 Simulated values (blue) of **a)** 30, **b)** 10, **c)** 5 and **d)** 2.5 mm sample drying characteristics compared to experimental results (red) at test temperature of 150 °C

heat transfer coefficient and the parameters related to the thermal conduction within the sphere.

4.1.2 Prediction of temperature dependence on drying performance

In order to quantify the particular features of drying kinetics, another computation was conducted at the same temperature range with the interval of 10 °C. The initial water percentage was assumed to be 51.3%, a value averaged over multiple experimental attempts on B2013 coal. The selected parameters are presented in Table 2.

The time of drying t_{dry} predicted by the simulation inclines sharply with the decrease of steam temperature, especially in the vicinity of 100 °C. For instance, temperature drop from 120 to 110 °C induces the extension of the drying process by

76%. The drying rate $(dX/dt)_{max}$ achieves peak value at the temperature of 170 °C. This value was simulated during the period, when dewatering is the most intense – the constant drying rate period (CDRP). The duration of this stage, t_{CDRP} was expected to last from 1.7% (170 °C) to 8.9% (110 °C) of the entire drying time. This relatively short period of the process has a decisive impact on the final effect of drying, what is displayed in section 4.2.2. The increase in the center temperature of over 100 °C, triggered by the complete evaporation of the free water in the sample, happens around half of the total time for higher steam temperatures and reduced to 1/3 when approaching the saturation temperature. It is marked as t_{free} . The largest gap between the temperatures of the surface and center ($\Delta T_{1,51,max}$) was computed at 32.3 °C, while in the opposite case it was as low as 1.8 °C. Therefore, the objects dried at high temperatures, what results in considerable

Table 2 Prediction of drying for 10 mm sample

T [°C]	t_{dry} [min]	t_{CDRP} [min]	$(dX/dt)_{\text{max}}$ [s ⁻¹]	t_{free} [min]	$\Delta T_{1,51,\text{max}}$ [°C]
170	62.6	1.0	8.89	24.2	32.3
160	74.1	1.5	7.31	27.9	26.2
150	90.9	2.6	5.83	33.4	20.6
140	117.0	4.5	4.45	39.4	15.3
130	162.5	7.2	3.18	51.0	9.7
120	256.5	12.5	2.02	70.2	5.0
110	450.2	40.1	0.96	129.8	1.8

thermal stresses, are more exposed to the hazard of structure deformation, what was illustrated in the video analysis included in the previous study [18].

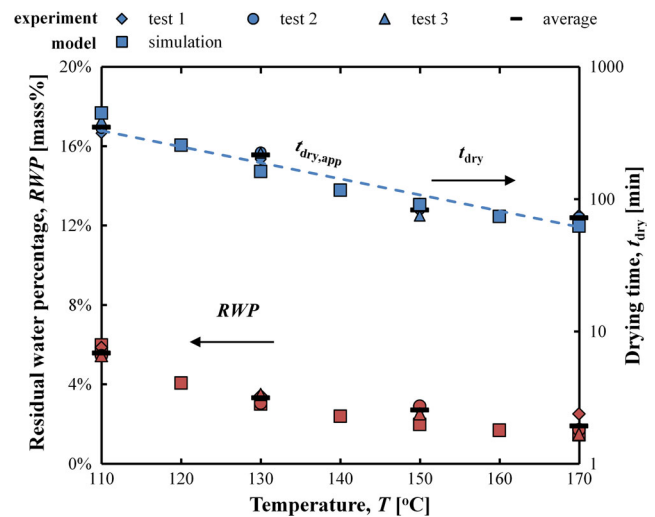
An analogical juxtaposition of the parameters for the drying of the 5 mm sample is gathered in Table 3. The time required for drying is around 3 times shorter, regardless of the gas temperature. The constant drying rate period occupies a similar part of the entire process (3.0% to 8.2%), however, the peak speed in dewatering is 2.5 times higher than of a larger object. The evaporation of the free water in the case of the 5 mm sample at 120 °C takes as much time as the analogical process conducted at 170 °C for the 10 mm object. Due to the smaller dimensions of the 5 mm sample, heat is transported through the sample much faster, what reduces the maximal level of the temperature gradient and limits the destructive impact of thermal stress on the coal structure.

4.1.3 Quantitative verification of numerical computations

In order to comprehensively analyse the coherence of the computational and empirical results, a summary of the values attained at the end of drying, total time of drying and residual water percentage, was prepared for the 10 mm sample in Fig. 6. The simulated results (square marker) are given for the entire temperature range with an interval of 10 °C, while three representative experimental cases and the averaged

Table 3 Prediction of drying for 5 mm sample

T [°C]	t_{dry} [min]	t_{CDRP} [min]	$(dX/dt)_{\text{max}}$ [s ⁻¹]	t_{free} [min]	$\Delta T_{1,51,\text{max}}$ [°C]
170	21.9	0.7	22.24	8.4	22.5
160	26.0	0.9	18.31	9.6	18.1
150	29.2	1.2	14.63	11.5	13.8
140	41.1	1.9	11.20	13.7	9.3
130	51.7	3.0	8.02	18.0	5.7
120	89.3	5.3	5.09	25.4	3.0
110	144.1	11.9	2.42	48.7	1.1

**Fig. 6** Residual water and drying time against drying temperature of 10 mm sample

value those from Ref. [16] are presented only for the conditions applied in the tests.

The experimental attempts served to formulate the equation, which was applied in the model for the estimation of the residual amount of water with regard to the drying temperature. Hence, a good agreement was achieved. In the case of the drying time, numerical values oscillated around the empirical results as well as the dashed line, which represents the approximation equation (Eq. 24) for the time of drying proposed in the previous work of the authors [18].

$$t_{\text{dry,app}} = 10^7 e^{-0.028T-7.238} \quad (24)$$

The empirical results of the drying time t_{exp} from Fig. 6 are shown altogether with their standard deviations $s(t_{\text{exp}})$ in Table 4. With reference to the values of t_{exp} , the root-mean-square error related to both approximation $R(t_{\text{dry,app}})$ and model $R(t_{\text{dry}})$ was evaluated. The coherence of the empirical results increases with the rise of the drying temperature. Similarly, the approximated and numerical results evince greater consistency with the experiment, however, the simulation offers precise prediction only for higher temperatures. The case of 110 °C was overshoot by the model, whereas drying in 130 °C lasted longer than the one predicted from the simulation.

4.2 Simulation of multi-particle drying in superheated steam

4.2.1 Drying of various coal assortments

The coal input to the grinder, which supplies the dryer, comes in various size assortment. As demonstrated in Fig. 5, drying time significantly decreases with the decline in object diameter. Hence, the energy consumed by the grinder on granulating

Table 4 Accuracy of drying time prediction

T [°C]	t_{exp} [min]	$s(t_{\text{exp}})$ [min]	$t_{\text{dry,app}}$ [min]	$R(t_{\text{dry,app}})$ [min]	t_{dry} [min]	$R(t_{\text{dry}})$ [min]
170	76.0	73.1	68.0	3.3	61.6	11.3
150	81.1	92.7	74.8	7.4	107.8	25.9
130	200.0	226.5	224.2	12.0	188.7	30.7
110	316.8	346.0	394.0	31.8	330.3	38.7

the fuel entails reduction of time, and thus energy, required for the operation of the dryer. The present study investigates the latter component of this interdependence.

The diameters of lignite spheres were assumed to fit the Rosin-Rammler equation, applied frequently to describe size distribution in fragmented minerals [24, 25]:

$$f(d) = 100 \times e^{-\left(\frac{d}{d_e}\right)^B} \tag{25}$$

In the formula above, $f(d)$ stands for a mass percent ratio of particles of diameter higher than d to total mass of the lignite group, d_e is a characteristic particle size for the particular group and B is a uniformity constant equal to 1 [15]. Due to the asymptotical character of Eq. 25 which tends to 0 as the diameter tends to infinity, the d_{max} value is introduced to represent the size over which the particles account for 1% of the mass distribution. Hence, to simplify the calculation, the mass percent ratio is divided into 10 subgroups. The derivative of $f(d)$ is presented for the case of $d_{\text{max}} = 80$ mm in Fig. 7.

Particles larger than 80 mm are not taken into account, subgroup 1 represents 9% of the total mass distribution, while subgroups 2–10 stand for 10% each. The square markers in the bottom axis illustrate the mean particle diameters in the particular subgroups.

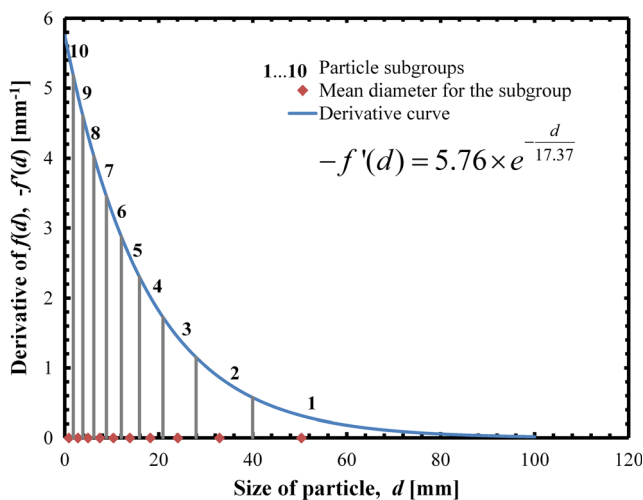


Fig. 7 Assumed size distribution of particles for $d_{\text{max}} = 80$ mm

Three scenarios of size distribution in the lignite batch exposed to the superheated steam were taken into consideration. The maximum diameter values of “fine”, “medium” and “thick” lignite groups were 40, 80 and 300 mm, respectively, what corresponds to the industrial practice of the Belchatow coal producer [26, 27]. The representative values for corresponding subgroups are shown in Table 5.

In Fig. 8, for the first 60 min of the process, the moisture content and drying rate of the multi-particle simulation for medium coal is plotted alongside the moisture content curves for the particular subgroups. The stepwise decline of the drying rate corresponds to the values attained by the samples of particular size at the subsequent stages of the process.

The visualized drying process of the particle grouped defined in the size quality, illustrated as the curves of the drying rate along the moisture apparent content, is presented in Fig. 9. The composition of the coal batch strongly influence the drying rate [28]. The dominant content of the smaller samples boosts the peak speed of the dewatering, determining the shape of the correlation curves. The computational graphs display irregularities, which were caused by a series of falling droplets formed from the water on the surface. Such a phenomenon, specific for the objects of around 30 mm and higher [19], occurred rarely in the drying of other samples [18]. The

Table 5 Representative diameters for subgroups in multiple drying cases

Scenario	Fine [mm]	Medium [mm]	Thick [mm]
d_{max}	40	80	300
Subgroup 1	25.19	50.38	188.95
Subgroup 2	16.48	32.96	123.59
Subgroup 3	12.04	24.08	90.31
Subgroup 4	9.12	18.24	68.39
Subgroup 5	6.94	13.88	52.02
Subgroup 6	5.19	10.39	38.95
Subgroup 7	3.74	7.48	28.06
Subgroup 8	2.50	5.00	18.74
Subgroup 9	1.41	2.82	10.59
Subgroup 10	0.45	0.89	3.34

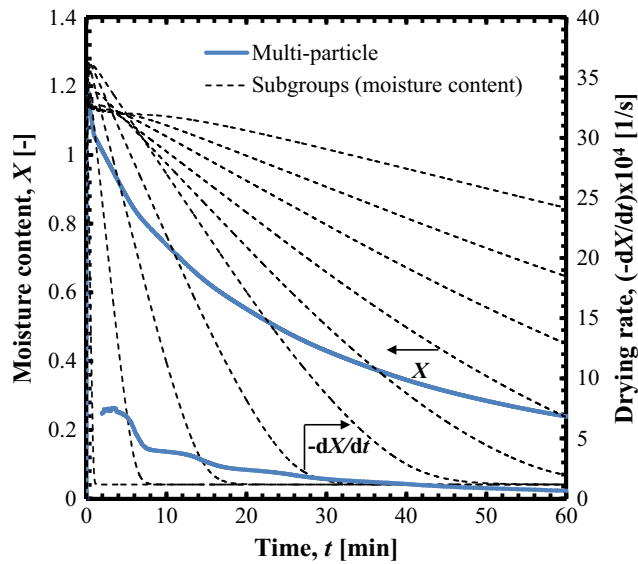


Fig. 8 Correlation of individual and multiple drying curves

analysis of the potential benefits in terms of calorific value, with reference to diverse multi-drying scenarios, are given in section 4.2.2.

4.2.2 The influence of drying on the efficiency of power generation

Two parameters were used to describe the drying impact on the optimization of power generation: thermal efficiency and carbon dioxide emission per generated unit of electricity. For the sake of the optimization analysis, a variable of water share, is introduced in Eq. 26. It expresses the absolute share of water within coal in the particular moment, unlike previously

discussed water percentage relating to the initial mass of coal before drying.

$$WS^i = \frac{m_w^i}{m^i} \cdot 100 = \frac{m_w^i}{m_w^i + m_c} \cdot 100 \tag{26}$$

In order to quantify those magnitudes, a brief insight into the coal composition is required. Table 6 contains the major components of B2013 lignite, relevant to the present analysis. The share of carbon and hydrogen was reported by a commissioned investigation with respect to coal deprived of water content (“dry coal” column) and recalculated to as-received state (“raw coal”). The structural division into the dry and liquid part of lignite is shown in Fig. 10.

The calculation of carbon dioxide emission relates to the stoichiometry of carbon combustion. Every 12 kg of carbon binds with oxygen to form 44 kg of CO₂.

Basing on the assumption that the carbon in the lignite is subject to complete combustion, the emission of CO₂ per kilogram of lignite is formulated as:

$$\{CO_2\}_{kg}^i = \frac{44}{12} C\%_d (1-WS^i) \tag{27}$$

where WS represents a variable of water share that decreases during drying.

Emission of carbon dioxide needs to be related to energy generation. Two indicators are commonly used to describe the thermal effect of fuel combustion. The higher heating value (HHV) represents the total amount of heat produced from the mass unit fuel with the assumption of no heat losses on the evaporation of water present in the fuel or produced parallel to combustion. Basing on the HHV value at the air-dried state, the parameter related to the dry state is:

$$HHV_d = \frac{HHV_{ad}}{1-WS_{ad}} \tag{28}$$

The HHV and water share for the air-dried B2013 coal are 19.08 MJ kg⁻¹ and 14.6 mass%, respectively, what results in HHV at 22.34 MJ kg⁻¹ for the dry coal. Therefore, the formula for the higher heating value of lignite during the drying process is shown in Eq. 29:

$$HHV^i = HHV_d (1-WS^i) \tag{29}$$

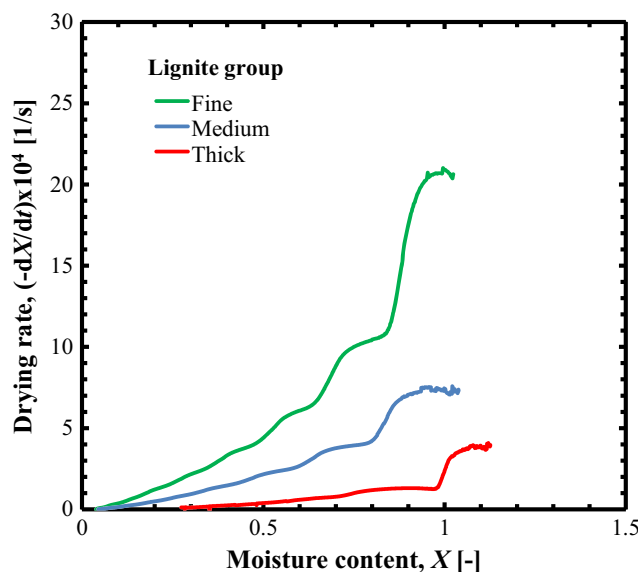


Fig. 9 Decline in drying rate for different coal groups

Table 6 Selected components of B2013 lignite

Component	Dry coal [mass%]	Raw coal [mass%]
water share WS	–	51.60
carbon C%	56.90	27.54
hydrogen H%	4.51	2.18
remaining dry part	38.59	18.68

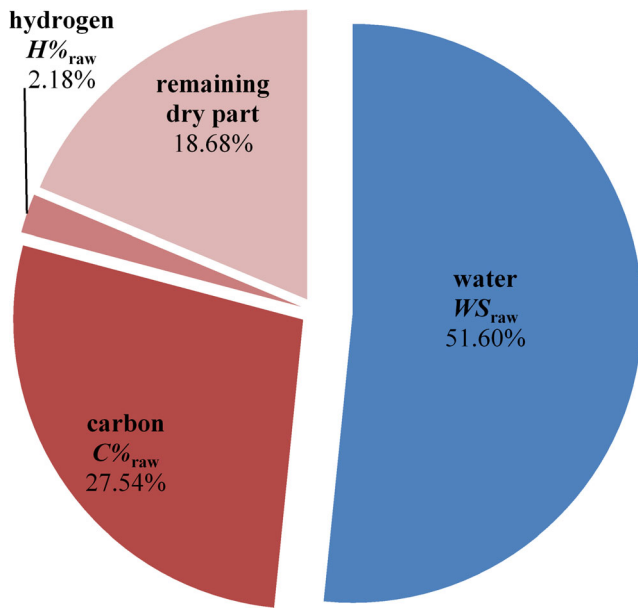


Fig. 10 Division of B2013 lignite into dry and liquid parts

The lower heating value (*LHV*), on the other hand, might be expressed as *HHV* less the heat needed for inherent moisture evaporation and water synthesized from hydrogen within dry coal. Given that 4 kg of hydrogen takes part in the synthesis of 36 kg of water, *LHV* with regard to coal in the drying process might be expressed as shown in Eq. 30.

$$LHV^i = HHV^i - L[WS^i + 9H\%_d(1-WS^i)] \quad (30)$$

Electricity generation per mass unit on fuel with certain *LHV* is directly proportional to thermal efficiency.

$$E^i_{kg} = LHV^i \times \eta_{LHV,raw} \quad (31)$$

Subsequently, the Eq. 32 formula presents carbon emission per generated kilowatt-hour:

$$\{CO_2\}^i_{kWh} = \frac{\{CO_2\}^i_{kg}}{E^i_{kg}} \times 3.6 \quad (32)$$

For the purposes of this study, it should be recognized that power generation companies often refer to *LHV* of applied fuel and calculate thermal efficiency based on this parameter, while in the research publications [29, 30], correlation between emission ratio and thermal efficiency rely on *HHV*. Therefore, thermal efficiency on *HHV* with regard to the one on *LHV* might be expressed as:

$$\eta^i_{HHV} = \frac{LHV^i \times \eta_{LHV,raw}}{HHV^i} \quad (33)$$

The changes in higher and lower heating value against declining water percentage are presented in Fig. 11. Data points are distributed every 5% of *WS*, with the exception of the one,

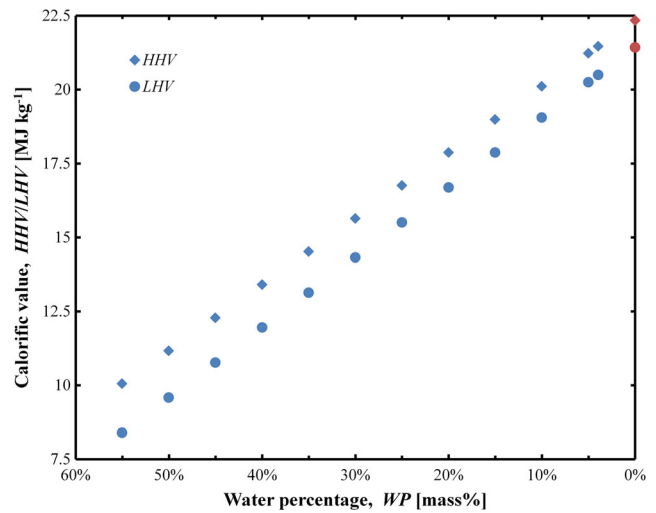


Fig. 11 Increase in calorific value due to drying

which marks 3.94%, a residual water share (equivalent to the residual water percentage of 1.98%) for the superheated steam drying at 150 °C. The initial gap between *HHV* (10.21 MJ kg⁻¹) and *LHV* (8.56 MJ kg⁻¹) decreases as the drying progresses, reaching a minimum value of 0.97 MJ kg⁻¹ at the end of drying. This final difference is attributed mostly to hydrogen content in dry coal part, as the theoretical margin (marked in red) for the completely dewatered lignite becomes 0.92 MJ kg⁻¹.

Enhancement in calorific value by means of drying involve economic and ecological benefits. Efficiency data provided by the electricity producer [31] relates to the *LHV* of raw lignite, what might be supported by information from the Belchatow power plant boilers manufacturer [32], providing data on the efficiency of the boiler accompanied by the *LHV* of supplying coal at the level of 8 MJ kg⁻¹. On this assumption, a chart in Fig. 12 was prepared describing the reduction of the CO₂ unit

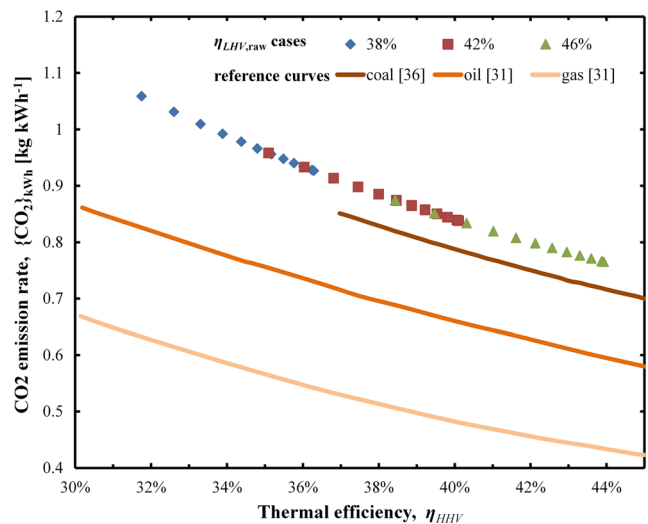


Fig. 12 Relation between plant thermal efficiency and CO₂ emission rate [29, 34]

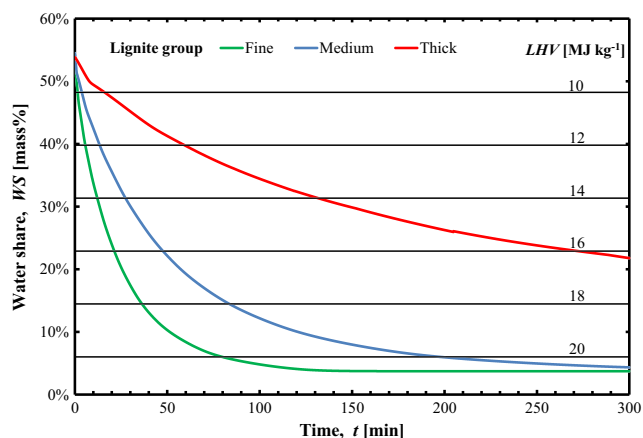
Table 7 Reference cases applied to CO₂ reduction analysis [31, 33]

Case	Thermal efficiency (LHV, raw coal)	Referring to Power Generation Unit	Electrical power output	Commissioned
Case 1	38%	Belchatow No. 1–12	370 MW	1980s
Case 2	42%	Belchatow No. 14	858 MW	2011
Case 3	46%	Kozienice No. 11	1075 MW	2017

emission caused by drying. The horizontal axis represents thermal efficiency recalculated to HHV according to Eq. 33. Three cases, gathered in Table 7 are included with regard to the net thermal efficiency of the power generation unit. Note that Cases 1 and 2 refer to lignite power plants, while Case 3 to the bituminous power plant.

Particular data points in each case are placed in the same water share interval as in Fig. 11: beginning with 55% on the left-hand side and descending to 5% and 3.94% on the right. The level of carbon dioxide emission for raw coal in Case 1 is 1.054 kg kWh⁻¹, a value compatible with data provided by the Belchatow power plant (1.069 kg kWh⁻¹ on average in 2015) [35]. Analogical values for Cases 2 and 3 are 0.954 and 0.871 kg kWh⁻¹. The total decline in the emission rate is 12.1% below the initial level, regardless the case. However, the distribution of data becomes denser as the water content drops, so it can be found out that the greatest profit for environmental efficiency is achieved in the early period of drying. The reference curves represent the carbon intensity along thermal efficiency for bituminous coal, oil and natural gas. Altogether with the correlation modelled hereby for lignite, they fit to the tendency that lower CO₂ emission levels are characteristic for fuels of higher hydrogen-to-carbon ratio (regarding dry part).

Figure 13 illustrates the simulated progress of drying for 3 batch compositions introduced in section 4.2.1, related to the boost in lignite lower heating value. The biggest enhance in the quality of this fuel is achieved in the initial period of drying. Given 8.56 MJ kg⁻¹ as raw coal's LHV, doubling the

**Fig. 13** Increase in LHV related to size composition of lignite batch dried at 150 °C

calorific value of Mixtures 2–4 (mass share of 30 mm samples at 10% or less) takes around 30 min for fine, 60 min for medium and over 400 min for thick coal. The differences extend as the drying continues, with regard to size distribution. For instance, whether the objective is to reach 18 MJ kg⁻¹ (WS≈14%, WP≈8%), a time interval between fine and medium coal is 47 min. However, the time required for raising LHV to 20 MJ kg⁻¹ (WS≈6%, WP≈3%), is 80 min in the case of the fine coal and almost 200 min for the medium one.

In conclusion, improving the quality of lignite and applied power generation technology might be beneficial in terms of ecology, nevertheless, the thermodynamic and financial costs of such efforts should also be taken into account. Therefore, an optimization of power generation unit (in particular fuel preparation devices: grinder and dryer), the general idea of which was proposed in the previous study [36], needs to be performed with regard to available industrial appliances.

5 Conclusions

Numerical modelling was used to simulate superheated steam drying for single and multiple samples made of Belchatow lignite, as an extension of the earlier work, concerning singular particles only [16]. The results of the investigation were presented in the form of drying charts containing experimental and computational curves as well as quantitative comparisons between those two data acquisition methods.

The application of multi-particle modelling was adapted in order to reflect a real operating mode of the drying system. By such means, a computational device is offered to calculate the time of drying for the demanded heating value of fuel. As a consequence, knowledge about dryer operational characteristics, may lead to heat input estimation. Taking into consideration several cases of fuel input composition, reflecting the actual assortments utilized in the Polish lignite industry, the potential enhancement of coal utilization effectivity was evaluated. The initial period of drying was found to be decisive in upgrading the quality of the fuel.

Further studies, complemented with the analysis of grinder energy demand as a function of coal fragmentation, may apply for the optimization of the drying system. Such works could also include intermediate scenarios, where different

assortments are mixed prior to input or the effect of sieving the most thick coal subgroups.

Acknowledgements The present study was financially supported by the Japan Coal Energy Center (JCOAL), the Polish National Centre for Research and Development (NCBR Project: I_POL-JAP, SSD-4-LRC) and also partially by the Polish Ministry of Science and Higher Education (Grant AGH No. 11.11.210.312).

Compliance with ethical standards

Conflict of interests On behalf of all authors, the corresponding author states that there is no conflict of interest.

Open Access This article is distributed under the terms of the Creative Commons Attribution 4.0 International License (<http://creativecommons.org/licenses/by/4.0/>), which permits unrestricted use, distribution, and reproduction in any medium, provided you give appropriate credit to the original author(s) and the source, provide a link to the Creative Commons license, and indicate if changes were made.

References

1. Patrycy A (2011) Wpływ produkcji energii elektrycznej w źródłach opalanych węglem brunatnym na stabilizację ceny energii dla odbiorców końcowych. *Górnictwo i Geoinżynieria (AGH J Min Geoengin)* 35:249–260 (in Polish)
2. Sa-Adchom P, Swadisevi T, Nathakaranakule A, Soponronarit S (2011) Mathematical model of pork slice drying using superheated steam. *J Food Eng* 104:499–507. <https://doi.org/10.1016/j.jfoodeng.2010.12.025>
3. Liu Y, Kansha Y, Ishizuka M, Fu Q, Tsutsumi A (2015) Experimental and simulation investigations on self-heat recuperative fluidized bed dryer for biomass drying with superheated steam. *Fuel Process Technol* 136:79–86. <https://doi.org/10.1016/j.fuproc.2014.10.005>
4. Morey RV, Zheng H, Kaliyan N, Pham MV (2014) Modelling of superheated steam drying for combined heat and power at a corn ethanol plant using Aspen Plus software. *Biosyst Eng* 119:80–88. <https://doi.org/10.1016/j.biosystemseng.2014.02.001>
5. Hausbrand E (1924) Drying by means of air and steam. *J Soc Chem Ind* 43:919. <https://doi.org/10.1002/jctb.5000433706>
6. Wenzel L, White RR (1951) Drying Granular Solids in Superheated Steam Engineering development. *Ind Eng Chem* 43:1829–1837
7. Yoshida T, Hyodo T (1970) Evaporation of water in air, humid air, and superheated steam. *Ind Eng Chem Process Des Dev* 9:207–214
8. Potter OE, Beeby CJ, Fernando WJN, Ho P (1984) Drying brown coal in steam-heated steam-fluidized beds. *Dry Technol* 2:219–234
9. Hoehne O, Lechner S, Schreiber M, Krautz HJ (2009) Drying of Lignite in a Pressurized Steam Fluidized Bed—Theory and Experiments. *Dry Technol* 28:5–19. <https://doi.org/10.1080/07373930903423491>
10. Fushimi C, Kansha Y, Aziz M, Mochidzuki K, Kaneko S, Tsutsumi A, Matsumoto K, Yokohama K, Kosaka K, Kawamoto N, Oura K, Yamaguchi Y, Kinoshita M (2010) Novel Drying Process Based on Self-Heat Recuperation Technology. *Dry Technol* 29:105–110. <https://doi.org/10.1080/07373937.2010.482719>
11. Mujumdar AS (2006) Superheated steam drying. In: Mujumdar AS (ed) *Handb. Ind. Dry*, Third edn. CRC Press, Boca Raton, pp 439–452
12. Tang Z, Cenkowski S, Muir WE (2004) Modelling the Superheated-steam Drying of a Fixed Bed of Brewers' Spent Grain. *Biosyst Eng* 87:67–77. <https://doi.org/10.1016/j.biosystemseng.2003.09.008>
13. Chen Z, Wu W, Agarwal PK (2000) Steam-drying of coal. Part 1. Modeling the behavior of a single particle. *Fuel* 79:961–973
14. Kiriyama T, Sasaki H, Hashimoto A, Kaneko S, Maeda M (2013) Experimental Observations and Numerical Modeling of a Single Coarse Lignite Particle Dried in Superheated Steam. *Mater Trans* 54:1725–1734. <https://doi.org/10.2320/matertrans.M-M2013817>
15. Kiriyama T, Sasaki H, Hashimoto A, Kaneko S, Maeda M (2016) Size Dependence of the Drying Characteristics of Single Lignite Particles in Superheated Steam. *Metall Mater Trans E* 1:349–363. <https://doi.org/10.1007/s40553-014-0037-2>
16. Zakrzewski M, Sciazko A, Komatsu Y, Akiyama T, Hashimoto A, Kaneko S, Kimijima S, Szmyd JS, Kobayashi Y (2016) An experimental verification of numerical model on superheated steam drying of Belchatow lignite. *J Phys Conf Ser* 745:1–8. <https://doi.org/10.1088/1742-6596/745/3/032145>
17. Umar DF, Usui H, Daulay B (2005) Effects of Processing Temperature of Hot Water Drying on the Properties and Combustion Characteristics of an Indonesian Low Rank Coal. *Coal Prep* 25:313–322. <https://doi.org/10.1080/07349340500444554>
18. Komatsu Y, Sciazko A, Zakrzewski M, Kimijima S, Hashimoto A, Kaneko S, Szmyd JS (2015) An experimental investigation on the drying kinetics of a single coarse particle of Belchatow lignite in an atmospheric superheated steam condition. *Fuel Process Technol* 131:356–369. <https://doi.org/10.1016/j.fuproc.2014.12.005>
19. Zakrzewski M, Komatsu Y, Sciazko A, Akiyama T, Hashimoto A, Shikazono N, Kaneko S, Kimijima S, Szmyd JS, Kobayashi Y (2016) Comprehensive study on the kinetics and modelling of superheated steam drying of Belchatow lignite from Poland. *Mech Eng J* 3:1–12. <https://doi.org/10.1299/mej.16-00365>
20. Komatsu Y, Sciazko A, Zakrzewski M, Fukuda K, Tanaka K, Hashimoto A, Kaneko S, Kimijima S, Szmyd JS, Kobayashi Y (2016) Experimental and analytical evaluation of the drying kinetics of Belchatow lignite in relation to the size of particles. *J Phys Conf Ser* 745:32144-1–32144-8. <https://doi.org/10.1088/1742-6596/745/3/032144>
21. Patankar S V (1980) *Numerical Heat Transfer and Fluid Flow*. Hemisphere Publishing Corporation
22. Szargut J (1992) *Modelowanie numeryczne pól temperatury*. Wydawnictwa Naukowo-Techniczne (in Polish)
23. Allardice DJ, Chaffee AL, Jackson WR, Marshall M (2004) Water in Brown Coal and Its Removal. In: Li C-Z (ed) *Adv. Sci. Vic. Brown Coal*. Elsevier Ltd., Oxford, pp 85–133
24. Nsakala NY, Essenhigh RH, Walker PL (1978) Characteristics of chars produced from lignites by pyrolysis at 808 °C following rapid heating. *Fuel* 57:605–611. [https://doi.org/10.1016/0016-2361\(78\)90189-8](https://doi.org/10.1016/0016-2361(78)90189-8)
25. Scaroni AW, Walker PL, Essenhigh RH (1981) Kinetics of lignite pyrolysis in an entrained-flow, isothermal furnace. *Fuel* 60:71–76. [https://doi.org/10.1016/0016-2361\(81\)90035-1](https://doi.org/10.1016/0016-2361(81)90035-1)
26. PGE Górnictwo i Energetyka Konwencjonalna S.A. Sprzedaż węgla. Kopalnia Węgla Brunatnego Belchatów. <https://kwbbelchatow.pgegiel.pl/Oferta/Sprzedaz-węgla>. Accessed 18 Dec 2017 (in Polish)
27. PGE Górnictwo i Energetyka Konwencjonalna S.A. Oferta. Kopalnia Węgla Brunatnego Turów. <https://kwbturów.pgegiel.pl/Oferta>. Accessed 18 Dec 2017 (in Polish)
28. Komatsu Y, Sciazko A, Zakrzewski M, Fukuda K, Tanaka K, Hashimoto A, Kaneko S, Kimijima S, Szmyd JS, Kobayashi Y (2016) Experimental and analytical evaluation of the drying kinetics of Belchatow lignite in relation to the size of particles. In: *J. Phys. Conf. Ser.*, pp 1–8

29. Booras G, Holt N (2004) Pulverized coal and IGCC plant cost and performance estimates. *Gasif Technol*
30. Bilek M, Hardy C, Lenzen M, Dey C (2006) Life-Cycle Energy Balance and Greenhouse Gas Emissions of Nuclear Energy in Australia. Sydney
31. PGE GiEK S.A. Oddział Elektrownia Bełchatów - O oddziale. <https://www.elbelchatow.pgegiiek.pl/index.php/o-oddziale/>. Accessed 21 Mar 2017 (in Polish)
32. Sylwetki kotłów RAFAKO. <http://www.rafako.com.pl/produkty/kotly/sylwetki/kotly-pylowe-przeplywowe2>. Accessed 21 Mar 2017 (in Polish)
33. Mitsubishi Hitachi Power Systems Europe GmbH (2014) First Boiler Column Fixed at the Koźienice 11 Power Plant, pp 1–3
34. White D (2004) Reduction in Carbon Dioxide Emissions: Estimating the Potential Contribution From Wind-Power
35. Wskaźniki emisji za rok 2015. <https://www.elbelchatow.pgegiiek.pl/index.php/ochrona-srodowiska/wskazniki-emisji/>. Accessed 22 Mar 2017 (in Polish)
36. Komatsu Y, Sciazko A, Zakrzewski M, Akiyama T, Hashimoto A, Shikazono N, Kaneko S, Kimijima S, Szmyd JS, Kobayashi Y (2016) Towards the improvement of thermal efficiency in lignite-fired power generation: Concerning the utilization of Polish lignite deposits in state-of-the-art IGCC technology. *Int J Energy Res* 40: 1757–1772. <https://doi.org/10.1002/er.3548>